Variations in the optical and thermoelectric behavior of $ZnCo_2O_4$ nanostructures as a function of synthesis temperature

M. Asad [a], N.-ur-Rehman [a,*], N. Bano [b], S. M. Ali [b], K. Mahmood [c], A. Ali [c], M. Imran [d]

[a] *Institute of Physics, The Islamia university of Bahawalpur, Bahawalpur63100, Pakistan*

[b] *Department of Physics and Astronomy, College of Science, P.O. BOX 2455, King Saud University, Riyadh 11451, Saudi Arabia.*

[c] *Department of Physics, Government College University, Faisalabad, Pakistan*

[d] *Beijing Key Laboratory of Environmental Science and Engineering, School of Materials Science and Engineering, Beijing Institute of Technology, P.R. China*

Zinc cobalt oxide nanostructures were synthesized by electrochemical deposition of zinc-cobalt alloy at various bath temperatures (15, 30, 45 and 60 ˚C) and its hydrothermal oxidation at 100 ˚C. X-ray diffraction pattern and Raman spectroscopy data reveals the formation of spinal structure of $ZnCo_2O_4$. Photoluminescence spectra of the samples exhibit broad peaks with a red shift in the emission energy. Diffused reflectance spectroscopy measured the band gap of the synthesized materials; band gap is 3.06, 3.03, 3.02 and 2.99 eV, for samples electrodeposited at 15, 30, 45 and 60 ˚C, respectively. Optical conductivity of synthesized materials decreases with increasing deposition layers while reflectance shows opposite trend. Thermoelectric set up measures the change in potential difference through synthesized materials when different temperatures are applied and an increment in potential were observed. Seebeck co-efficient and power factor are also studied as function of bath temperature.

(Received August 29, 2024; Accepted October 21, 2024)

Keywords: Zinc cobalt oxide, Electrochemical deposition, Hydrothermal oxidation, Diffused reflectance, Thermoelectric properties

1. Introduction

The increase in population is responsible for the increase in demand for energy. However, 86% of the energy demand is fulfilled by the combustion of fossil-fuels. The limited availability of fossil-fuels in future, emission of toxic gases causing global warming and cost problems have led researchers to search alternative nontoxic, low-cost renewable resources [1-3]. Several renewable energy resources like solar, hydro, wind and Biomass are contributing to the society. In this particular scenario, thermoelectricity serves as method enabling the transformation of heat into electrically energy without moving parts. Even though thermoelectric devices fall significantly short of reaching 20% efficiency [4], their utilization remains inevitable due to the technology's indispensability. Thermoelectric devices not only generate energy but also reduce global warming (increasing on daily base due to liberation of heat from automobiles and industries etc.) without producing any negative impact. The effectiveness of thermoelectric devices is quantified by the dimensionless figure of merits (ZT) of the materials measured by, [ZT= (S^2 σT)/k] where 'S' represents Seebeck coefficient, 'σ' electrical conductivity, 'T' temperature, 'k' represents thermal conductivity and S2σ represents power factor, an influential criterion in the quest for efficient thermoelectric materials [5]. In order to achieve superior thermoelectric performance, the materials must exhibit minimal thermal conductivity 'k', heightened electrical conductivity 'σ' and significant thermopower 'S'; This objective can be accomplished through techniques such as nano-structuring, band manipulation, and the induction heavy elements via doping. Currently

* Corresponding author: naeem.rehman@iub.edu.pk
https://doi.org/10.15251/JOR.2024.205.745

conventional materials predominantly consist of intermetallic compounds based on heavy metals that are commercially available [6, 7]. Nevertheless, the utilization metallic materials are constrained by their restricted operational temperature range, susceptibility to oxidation in atmospheric conditions, environmental concerns regarding heavy elements, high toxicity and scarcity of resources. Due to the numerous limitations associated with the intermetallic compounds (like as Bi2Te3, PbTe, Cu2Te, and SnSe) there has been a significant surge of metal oxide base thermoelectric materials over the past few decades. Despite the fact that the metal oxide based thermoelectric materials exhibit less efficiency than intermetallic compounds, they have garnered significant research attention due to their appealing attributes including; robustness at elevated temperatures, nontoxicity, cost effectiveness and eco-friendliness [8-13]. During the period spanning from 1950 to the 1970 there was surge in exploration for oxide thermoelectric materials. Concurrently, researches in the United States delved into the intrinsic characteristics of grown oxide single crystals through the utilization of thermoelectric effects. Since the 1990, the pursuit of oxide thermoelectric materials, originating in Japan has expanded globally encompassing Europe, the United States, Asia and India. It has been documented that certain oxides may demonstrates parameters surpassing ZT >1, exceeding those of PbTe.

Thermoelectric oxides have long historic background. During the era between 1950 to the 1970 often referred to as initial surge, significant attention was devoted to exploring the thermoelectric characteristics of numerous straightforward conducting oxides such as CdO, NiO, ZnO, In2O3, SrTiO3, rutile-TiO2, SnO2, Cu2O and Fe3O4 were investigated in 1st Boom for the estimation of physical characteristics of like as effective mass of carriers [14-22]. The superconducting oxides (high Tc) like as La2CuO4, La-Ba-Cu-O, YBa2-Cu3O7-δ, and Tl-Ca-Ba-Cu-O, were investigated for thermoelectric properties in 2nd Boom [23-27]. Some other superconducting materials (high Tc) like as CaMnO3, Al doped ZnO and NaxCoO2 with excellent thermoelectric results were also documented by the Ohtaki and Terasaki [28-30]. The publication of these findings sparked resurgence in the exploration of thermoelectric oxides during 2000s, marking the advent of third wave. This period of heightened interest led to the discovery of Ca3Co4O9 and (La doped, Nb doped and electron doped) SrTiO3, through intensive investigative efforts into promising thermoelectric materials [31-35]. Fergus conducted an assessment of the thermoelectric characteristics of perspective oxides in 2012 predominantly focusing on bulk ceramics. This review encompassed materials such as Ca3Co4O9, NaxCoO2, SrTiO3, CaMnO3, and ZnO [36]. Lately several scholars have documented remarkable ZT values for ceramic oxides, for instance SrTi0.85Nb0.15O3 sintered alongside graphite flakes, demonstrate a ZT value of 1.4 at 1050K and Al doped ZnO sintered alongside reduced graphene oxides demonstrate a ZT value of 0.5 at 1100K [37, 38]. Despite the appealing nature of reported ZT values for serving as practical thermoelectric materials, their practical implementations remain elusive, likely owning to concerns regarding the reliability of the ZT values.

Among all these oxide materials [7, 39-41] which were investigated in previous years, $ZnCo_2O_4$ is one which has been documented for storage and catalytic investigation but not for thermoelectric applications. It's a ternary metal oxide alongside mixed valence, possessing a spinel cubic structure and falling with in the $Fd\bar{3}m$ space group. $ZnCo_2O_4$ has P-type behavior, with divalent Zn ions occupying tetrahedral sites and trivalent Co ions residing octahedral sites [6, 42]. The present study aims to estimate the thermoelectric characteristics of $ZnCo_2O_4$ synthesized at various temperatures.

2. Experimental procedure

Electrodeposition of metallic alloy followed by its oxidation process has been adopted to synthesize the zinc cobalt oxide thin films on copper substrate. For the purpose, $ZnCl_2$ and $CoCl_2$ were used as a source of zinc and cobalt sources in the solution, respectfully. In addition, dimethyl sulfoxide (DMS) was used as supporting electrolyte. At the end, Distilled water, Ethanol and acetone used for washing purpose.

A DC power supply was used as a current source to provide opposite polarities to copper substrate and reference graphite electrode. The copper substrate was cut in 1×3 cm^2 dimensions

and polished by sand papers of different grit sizes for removing oxidized surface layer and smoothness. After preparing the substrate, this was dipped in the prepared 80ml solution of $CoCl_2$ (0.1M) and $ZnCl_2$ (0.1M) in distilled water. The sample was prepared at a provided current density of 35 mA/cm^2. Four coatings were deposited on copper substrate for 15 minutes at 15, 30, 45 and 60 ˚C temperatures. After the deposition, each coating was dried by using hot air. Fresh solutions were used for the deposition of each layer. All these layers then oxidized at 100 ˚C by putting them in a stain less steel autoclave filled with distilled water. The autoclave was kept in the oven for duration of 12 hours in order to get complete oxidation of Zn-Co alloy coatings.

The structural study of the nanostructures was carried out by Bruker D8 x-ray diffractometer equipped with Cu-Kα radiations of 0.154 nm. The size and morphology have been studied by TESCAN Mira3 field emission scanning electron microscope Equipped with EDAX for elemental analysis of the nanostructures. Photoluminescence measurements to study optical emissions from the nanostructures were performed at room temperature by exciting the samples with 325 nm He–Cd laser line (Melles Griot Series 56) at 15 mW. The Raman spectra were achieved by a confocal mapping system having an excitation source of 632.8 nm. Thermoelectric measurements were carried out by using a self-made system. The electrical conductivity values were recorded by Hall system (Ecopia). Optical reflectance of the samples was studied with a JASCO (V-670) spectrophotometer.

3. Results and discussion

3.1. XRD analysis

XRD analysis was conducted to assess the phase, crystallinity and structure of the synthesized materials. As depicted in Fig. 1, XRD spectra exhibits discernible peaks at 31.2º, 36.6º, 38.5º, 44.8º, 55.6º, 59.3º, 65.2º, aligning with the (220), (222), (311), (400), (422), (511), and (440) crystal planes, respectively, thereby confirming the (Fd$\bar{3}$m space group) spinel structure of $ZnCo_2O_4$ (JCPDS 23-1390). The absence of additional peaks and sharpening of existing peaks serves as evidence affirming the exceptional crystalline quality and purity of the samples [43-47].

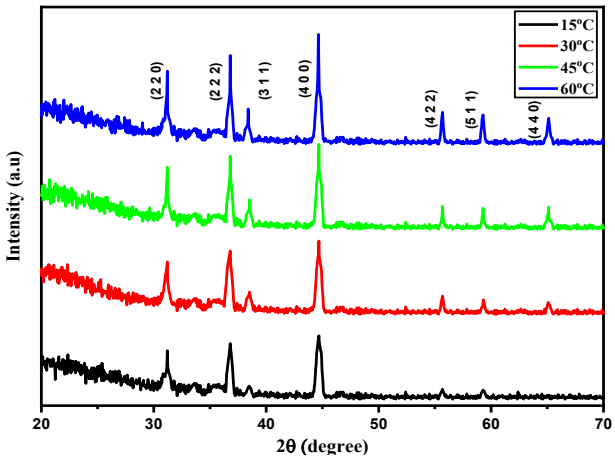

Fig. 1. XRD patterns of $ZnCo_2O_4$ nanostructures.

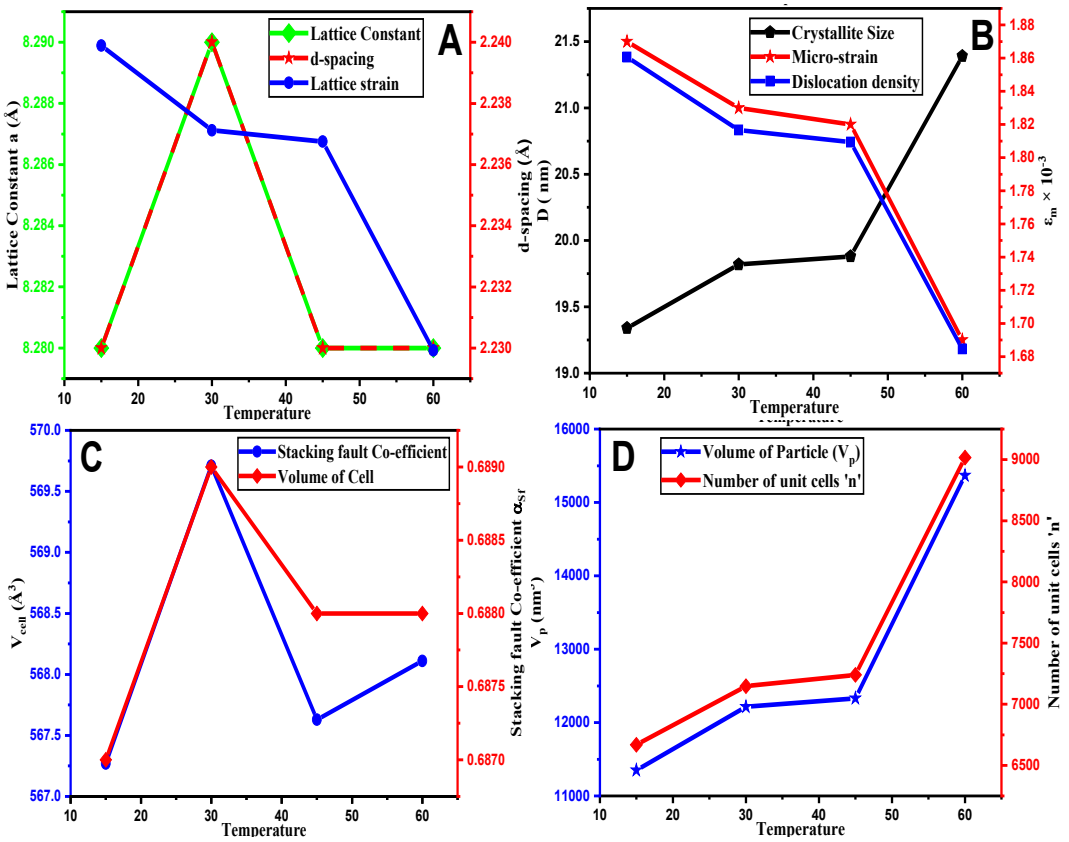

Fig. 2. (a) Lattice Constant (b) Crystallite Size, (c) Lattice Strain and (d) Cell volumes of the nanostructure.

The following formulas were employed to estimate the various parameters listed in the Table 1.

$$\text{d-spacing} \quad d = \frac{n\lambda}{2\sin\theta} \tag{1}$$

$$\text{Lattice constant} \quad a = d\sqrt{h^2 + k^2 + l^2} \tag{2}$$

$$\text{Volume of unit cell} \quad V_{cell} = a^3 \tag{3}$$

$$\text{Stacking fault } \alpha_{Sf} = \frac{2\pi^2}{45\sqrt{3}\,tan\theta} \tag{4}$$

where n represents diffraction order, θ diffraction angle, hkl miller indices, d inter-planar distances, V_{cell} volume of unit cell and α_{Sf} represents stacking fault [48, 49].

X-ray density can be defined and calculated by the following formula:

$$\text{X-ray density } (\rho_x) = \frac{ZM}{N_A V_{cell}} \tag{5}$$

'Z' represents number of molecules per unit cell in spinel structure, 'M' molecular weight of the samples, 'N_A' Avogadro's number (N_A = 6.02× 10^{23} mol^{-1}) and V_{cell} represents volume of cell.

The crystallite size, lattice strain, micro-strain and dislocation density were estimated by the below mentioned formulas [50, 51]:

Table 1. List of various estimated structural parameters as a function of synthesis temperature.

	15 °C	**30 °C**	**45 °C**	**60 °C**
Parameters				
D_{avg} (nm)	19.34	19.82	19.88	21.39
d-spacing (nm)	0.2233	0.2236	0.2233	0.2234
a (Å)	8.278	8.289	8.279	8.282
V_{cell} (Å^3)	567.27	569.71	567.63	568.11
ρ_x (g/cm^3)	5.789	5.764	5.785	5.780
$\delta \times 10^{-3}$ (nm^{-2})	2.674	2.546	2.531	2.185
$\varepsilon_L \times 10^{-3}$	5.435	5.292	5.272	4.906
$\varepsilon_m \times 10^{-3}$	1.872	1.831	1.822	1.692
α_{Sf}	0.687	0.689	0.688	0.688
V_p (nm^3)	11348.76	12216.19	12329.26	15367.25
N	6668.52	7147.53	7240.15	9016.55

$$\text{Crystallite Size } D = \frac{k\lambda}{\beta cos\theta} \tag{6}$$

$$\text{Lattice strain } \varepsilon_L = \frac{\beta}{4tan\theta} \tag{7}$$

$$\text{Micro-strain } \varepsilon_m = \frac{\beta cos\theta}{4} \tag{8}$$

$$\text{Dislocation density } \delta = \frac{1}{D^2} \tag{9}$$

'β' indicates FWHM and 'k' the shape factor. The volume of particle (V_p) and (n) number of unit cells per unit volume of cell were determined by following relations [52, 53]:

$$V_p = \frac{4\pi}{3}\left(\frac{D}{2}\right)^3 \tag{10}$$

$$n = \frac{\pi}{6}\left(\frac{D}{a}\right)^3 \tag{11}$$

where 'D' is crystallite size and 'a' represents lattice constant.

Fig. 2 depicts the variation in XRD parameters with temperature elevation. Higher temperatures lead to a reduction in atomic imperfections such as dislocation and strain. In contrast, the crystallite size, particle volume, and number unit cells all increase in tandem correspondingly to temperature elevation. These observed variations collectively indicate rise in temperature, resulting in enhanced crystallinity.

3.2. Raman analysis

Raman spectrums of $ZnCo_2O_4$ are shown in Fig. 3. The peaks that observed on 516-520 cm^{-1} are rich in cobalt samples. This is particularly a configuration of spinel structure compound having $Co^{2+}(Co2^{3+}O_4)$ in Co_3O_4 [54]. The peaks at 666 cm^{-1} that are observed due to the zinc oxide and also the peaks observed at 439 cm^{-1} are particularly shows zinc oxide wurtzite behavior [55]. The peak centered around 520 cm^{-1} is due to slight defects by tetrahedral Co site. As a result of octahedral O vibration, the broad peaks at 650-670 cm^{-1} can be observed. By substituting the atoms of zinc the peak of lower energy is observed which is due to the disorder in the spinel crystal structure locally [56]. The peaks that are observed around 514 cm^{-1} and 475 cm^{-1} are because of the combined vibrations of the ions of oxygen that are in motion in both tetrahedral and octahedral. Broadness of the bands is evident from the graph and the bands are not in accordance with the first-order phonons analyzed in a single-crystal [57]. Also, occurrence of the bands is

mainly due to multi-phonons vibrations. Increase of temperature shift the Raman bands towards lower frequency as can be seen in Figures 4.(a-d). This shifting of peaks is due to thermal expansion [58].

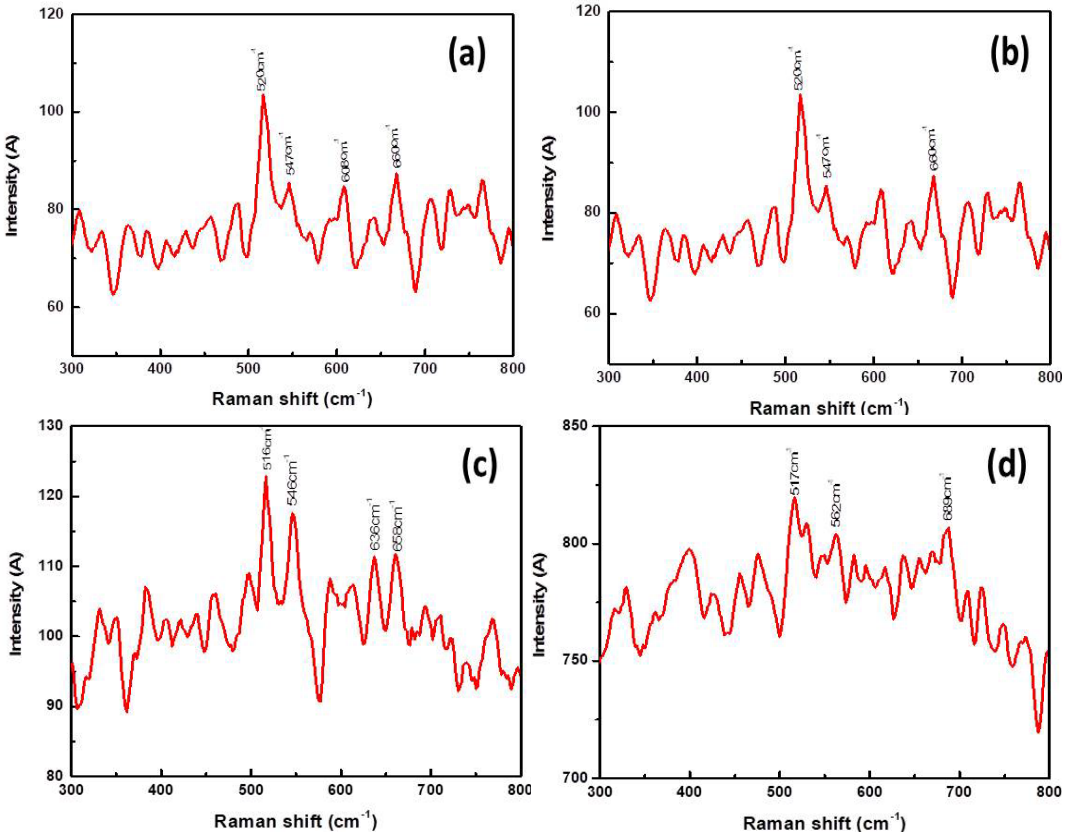

Fig. 3. Raman spetra of $ZnCo_2O_4$ sapmles synthesized at different temperatures (a) 15 C˚ (b) 30 C˚ (c) 45 C˚ and (d) 60 C˚.

3.3. SEM analysis

For the observation of grain size and crystal morphology of the grown samples SEM was used. Fig. 4 shows the SEM results of ZnCo2O4 films grown at different temperatures. The first sample is deposited at room temperature which indicates that some particles show needle liked shape and some particles shows nail like shape. The second sample is deposited at 30°C temperature which shows that by increasing the temperature particles of the film change their shape and shows a rod like morphology. Third sample deposited at 45°C temperature, which indicates that by gradually increasing the temperature the particles of the sample show grainy shape. Image of the fourth sample which deposited at 60°C of temperature shows that by increasing more temperature the particles of the film at some places show grainy shape and at some places these particles show needle like shape.

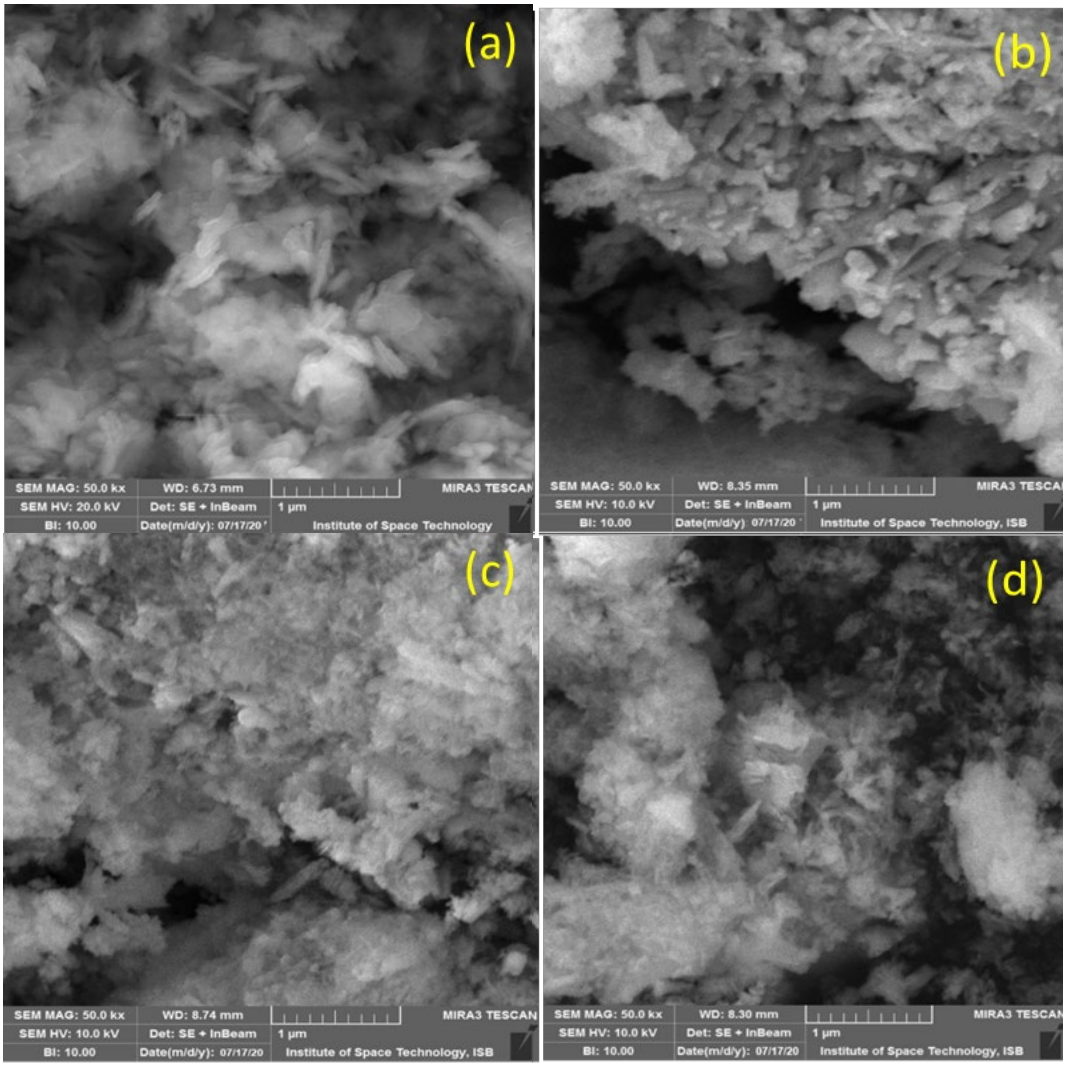

Fig. 4. SEM images of $ZnCo_2O_4$ nanostructures synthesized at different temperatures (a) 15 C˚ (b) 30 C˚ (c) 45 C˚ and (d) 60 C˚.

3.4. EDX analysis

Fig.5 shows EDX spectrum for zinc cobalt oxide samples. A different element of the samples is observed which indicates the confirmation of Zn, cobalt, and O contents and the presence of cobalt in zinc oxide particles. The peak clearly indicates the presence of zinc, cobalt and O and it is confirmed from the EDX spectra that at various temperature $ZnCo_2O_4$ nanostructures have been synthesized.

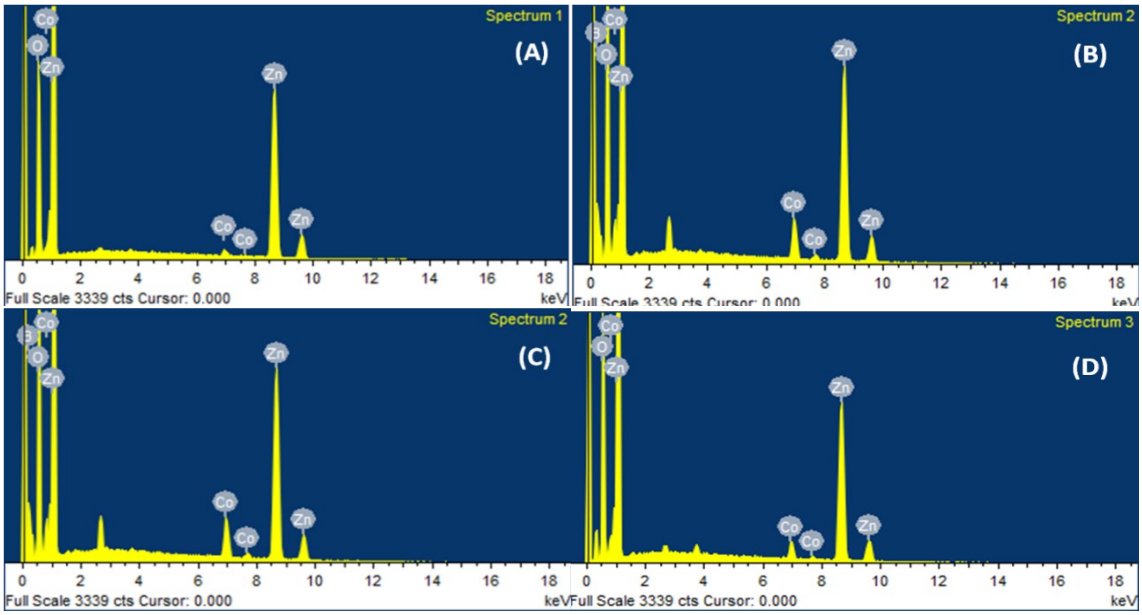

Fig. 5. EDX spectra of ZnCo2O4 samples synthesized at different temperatures (a) 15 C˚ (b) 30 C˚ (c) 45 C˚ and (d) 60 C˚.

3.5. Optical properties

PL analysis is sensitive way to analysis the extrinsic defects and intrinsic defects in the materials. It provides information for the energy states of defects and impurities even at much lower densities through which the structural defects can also be observed. It also provides additional information for the crystal quality of the grown films from different emissions. It is known that the emissions like green, yellow, violet, blue, red and orange produced due to the different kind of defects (Tarwal et al., 2014).

The PL spectra for the synthesized $ZnCo_2O_4$ films are shown in the Fig 6. At the temperature of 15°C the prepared sample shows a broad emission peak which corresponds to an energy band gap of 3.06 eV. At this photon energy the emission is observed due to the recombination of free excitons. The second sample which was grown at 30°C also exhibit only one emission around 3.03 eV which also have same origin as that of earlier one. The third sample prepared at 45°C, shows a similar behavior with an emission peak centered at 3.02 eV. The fourth sample which was synthesized at 60°C has energy band gap of 2.99 eV. It can be seen from all the samples that the defect related emission have only observed in the film which is deposited at very low temperature ~ 15ºC. As the temperature rises above the room temperature, the defects are removed from the crystals.

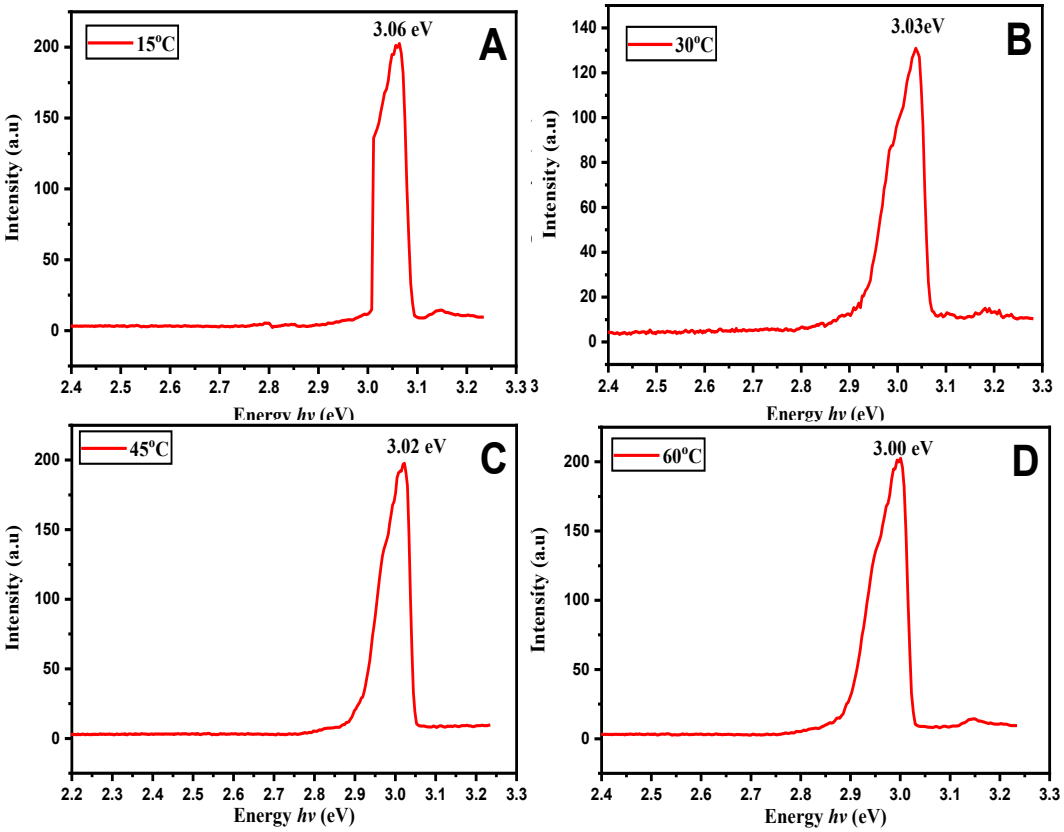

Fig. 6. PL spetra of $ZnCo_2O_4$ samples with estimated optical band gaps.

Optical behavior of the thin films was investigated by Diffused Reflectance Spectroscopy (DRS). Reflectance, absorption coefficient, band gap energy, optical conductivity through the materials, refractive index of all samples, extinction coefficient and optical dielectric constant have been calculated to study the response of nanomaterials against incident light. Band gap of these layers was calculated by Tauc plot using equation [59, 60]:

$$(\alpha h\nu) = K(h\nu - E_g)^{1/n}$$

where α, *hν,* E_g, K and n, are representing the absorption coefficient, photon energy, band gap energy, constant of proportionality and nature of transition (n = 2 for direct bandgap transition and n = ½ for indirect transition) respectively.

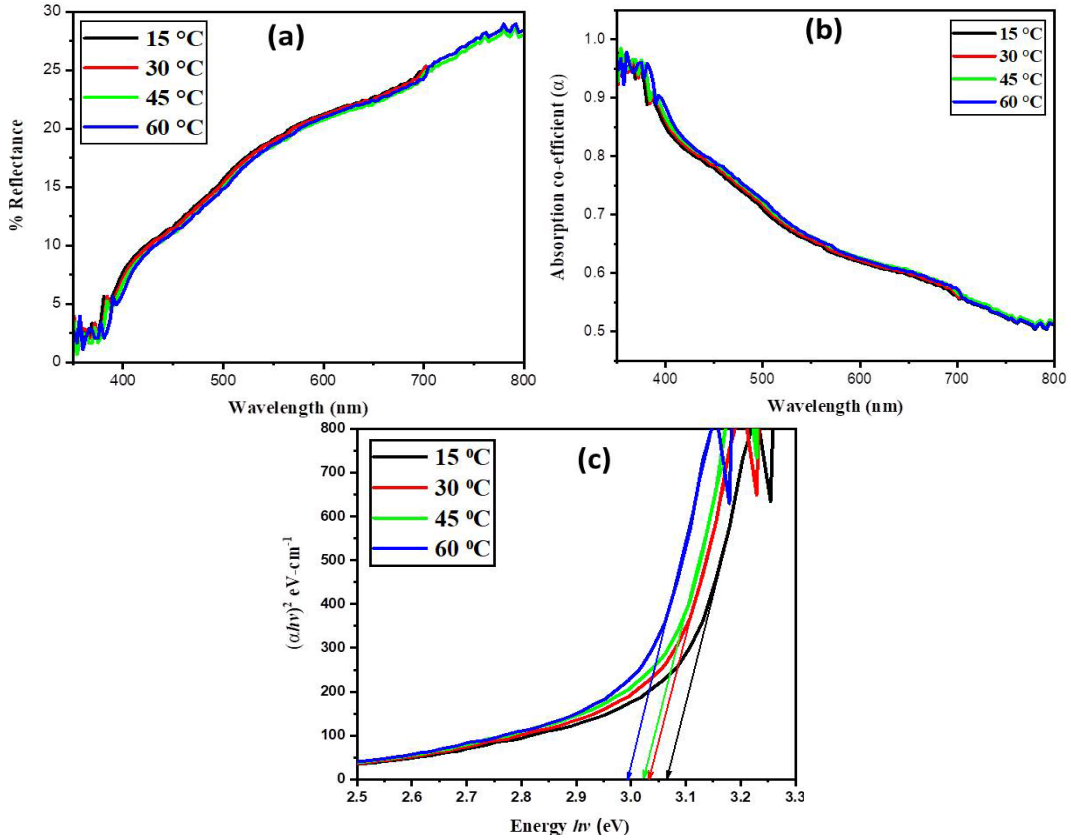

Fig. 7. (a) Reflection of the samples vs wavelength, (b) Absorption coefficient vs wavelength; (c) Band gap variation of different $ZnCo_2O_4$ samples.

It can be seen from figure 7(a), reflectance of the materials is decreasing to the smaller wavelength (high energy photons) which confirm that films are mostly responding in ultra violet and a little bit to visible region for the transmission of carriers from V_B to C_B. This behavior can be due to two reasons first is low carrier generation and second is strong bonding. However, reflectance increases towards high wavelength length which means only specific energy photons will participate in transmission. In the contrast absorption of the films is increasing towards smaller wavelength. The highest absorption is in the region of 375-380 nm and more charge carriers transfer in this region. From the figure 7(a), it can also be observed that intensity of absorption peaks is increasing and shifting towards higher wavelength (red shift). This type of behavior can be understood due to Local surface plasmonic resonance which be produced due to secondary phases of cobalt oxide [61-63]. However, absorption decreases towards further higher wavelength is decreasing because of low charge carriers to higher energy states of V_B and low energy photons. Growth temperature has a significant effect on the absorption as well as reflectance of the materials. As the growth temperature increase the absorption of materials increases and reflectance decreases with respect to each other [64, 65].

The band gap energy of the synthesized nanostructures was calculated by extrapolating $(\alpha h\nu)^2$ against $h\nu$ as shown in figure 7(b). A straight line was drawn from the slope of the graph and extended to touch the energy axis. The point where this straight line intersects the energy axis indicates the bandgap energy. The energy values at the intersection points for the samples deposited at 15, 30, 45 and 60 °C are estimated as 3.06, 3.03, 3.02 and 2.99 eV, respectively. The band gap of the nanomaterial films has exhibited a reducing trend from 3.06 eV to 2.99 eV. The decrease in band gap can potentially be attributed by the lattice distortion caused by the secondary/multiple phases of cobalt oxides. These phases introduce the additional energy levels in forbidden gap located below the C_B resulting in the decrease of band gap. Secondly metal clusters

formation during deposition and then oxidation creates local energy levels and surface plasmonic absorption which reduce the band gap [66, 67].

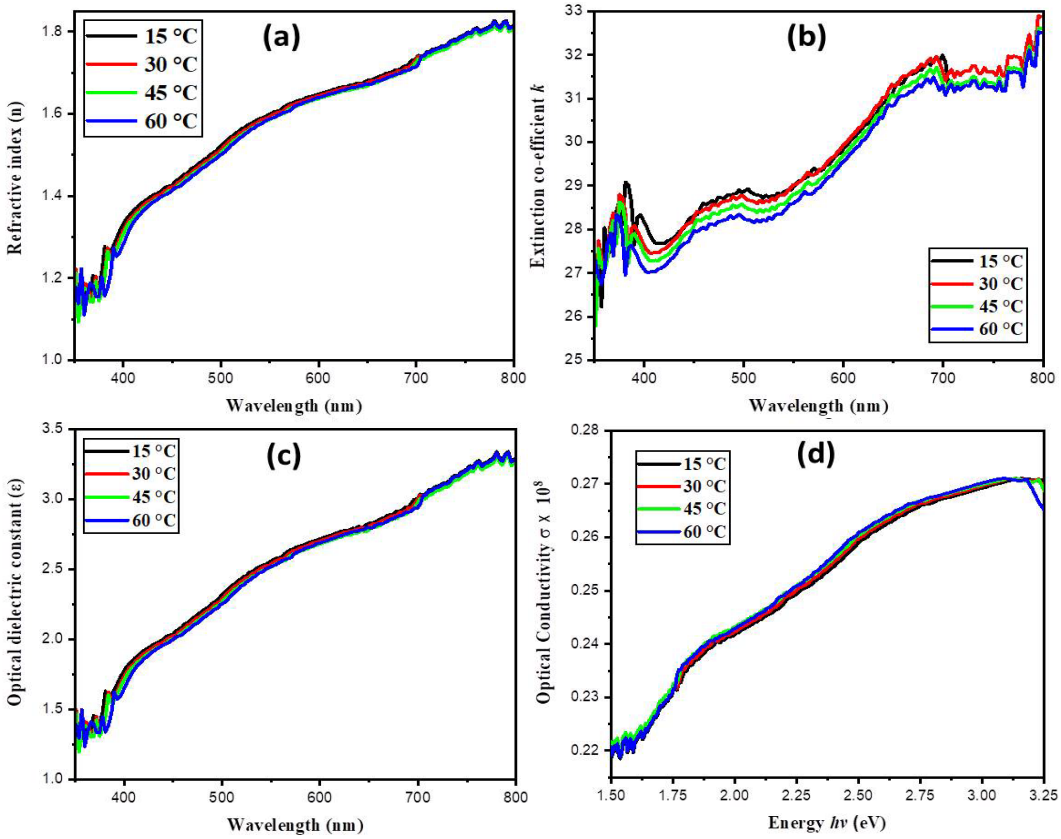

Fig. 8. (a) Refractive index, (b) Extinction coefficient, (c) Dielectric constant, (d) Optical conductivity of $ZnCo_2O_4$ samples.

Refractive index and extinction coefficient are to essential parameters of optical study of materials. These optical constant parameters have a great influence in optical uses mostly in optic devices.

The refractive index of the films was measured by reflectance using the relation [68]:

$$n = \frac{1 + \sqrt{R}}{1 - \sqrt{R}}$$

It can be seen from figure 8(a) that the refractive index is increasing towards higher values of wavelength. The refractive index varies as a function of wavelength, with its values increasing with wavelength in the visible region. However, in the UV and IR regions, it shows fluctuations. At some points, its values increase, while at others, they decrease. This can be attributed to the damping of thin films of Cobalt oxide and ZnO. Additionally, it can be noticed that the refractive index reduces with an increase in growth temperature, implying that the refractive index can be varied by adjusting the growth temperature [68, 69].

The extinction coefficient (k) is the imaginary part of complex refractive index ($n^* = n + ik$). It was calculated by Swanepoel method using following relation [70-73]:

$$k = \frac{\alpha\lambda}{4\pi}$$

Figure 8(b) Illustrates the increase in extinction co-efficient with respect to wavelength which highlights the surface evenness and homogeneity in particles causing the large scattering. Relative permittivity was estimated by using following relation:

$$\varepsilon_{\circ} = n^2$$

where $\varepsilon_{\circ}$ indicates optical dielectric constant also referred to as relative permittivity is increasing to the lower frequency of incident light. This increment to the lower frequency specifies the increase in polarization towards lower frequency. However, the decline in relative permittivity is attributed to the incapacity of electric charge carriers to keep pace with the oscillations of the applied ac electric field beyond specific critical frequency. Conversely elevated frequencies exhibit minimal optical dielectric constant, a crucial characteristic for the development of materials utilized in photonic and electro-optic devices. The increase in growth temperature reduces polarization due to miner phase transition [74].

Optical conductivity of the materials due photons of energy was calculated by applying refractive index and absorption coefficient in following relation [74]:

$$\sigma = \frac{\alpha n c}{4\pi}$$

Fig. 8(d) is elaborating the optical conductivity of the materials. It can be seen that optical conductivity of materials is increasing in visible region with rise of growth temperature. However optical conductivity is decreasing with increase of wavelength which elucidates that free carriers are affected by the traps which may present in band gap, in general decrease of photon energy reduces the optical conductivity. The optical conductivity is very high in UV visible region due to availability of free carriers produced by high energy photons [75].

3.6. Thermal properties

Thermoelectricity is renewable and low-cost energy resource it converts wasted heat into electrically energy through Seebeck co-efficient. When temperature difference is adjusted across the thermoelectric material, then potential difference is established for the diffusion of carrier across the material [76, 77]. The thermoelectric performance of the materials depends on the dimensionless quantity known as “figure of merits “ZT”.

$$ZT = \frac{S^2 \sigma T}{\kappa}$$

where “S”, “σ”, “T” and “κ” indicates the Seebeck co-efficient, electrical conductivity, temperature and thermal conductivity respectively. The product of ($S^2\sigma$) is defined as power factor and (κ) as sum electronic and lattice thermal conductivity [77, 78]. High value of power factor is increases the value of ZT which is responsible for high performance of thermoelectric material [79].

Seebeck co-efficient is the ratio of the potential difference to the temperature due to which that is adjusted across the contacts:

$$\Delta S = \frac{\Delta V}{\Delta T}$$

where ΔS, ΔV, and ΔT, represent Seebeck co-efficient, change in potential and change in temperature respectively.

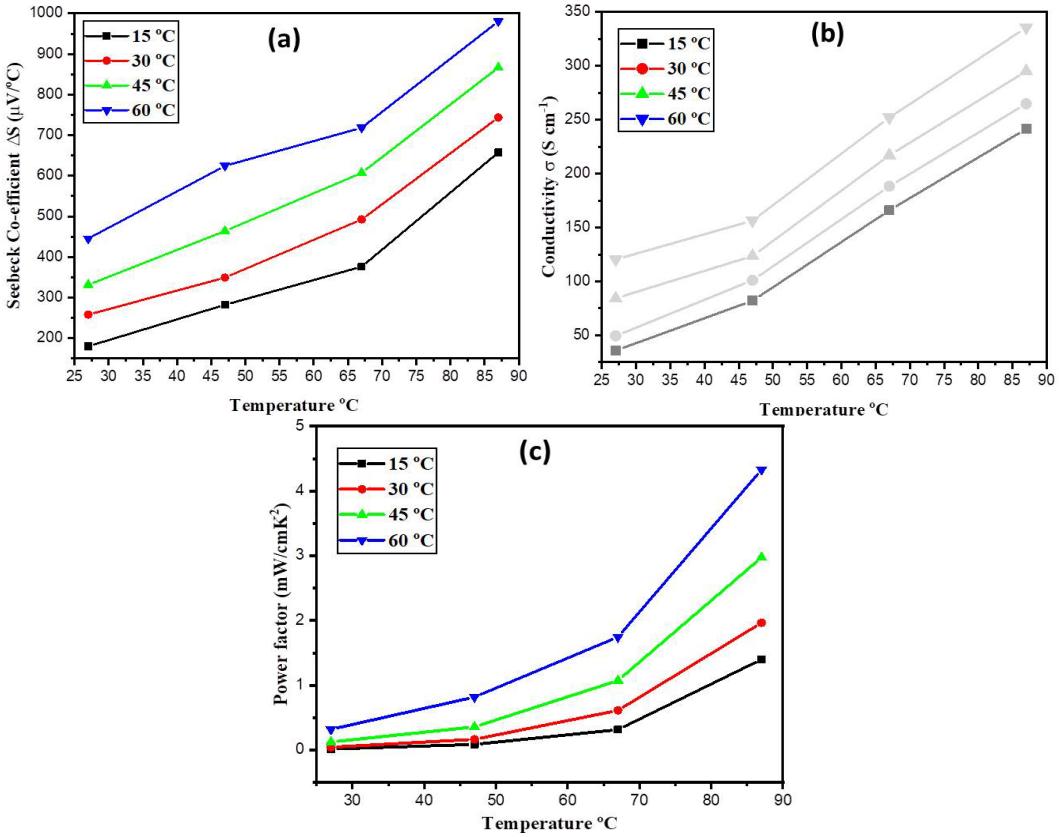

Fig. 9. (a) Seebeck Coefficient vs Temperature, (b) Electrical conductivity vs temperature, (c) variation in power factor with temperature.

Table 2. List of thermoelectric parameters for different $ZnCo_2O_4$ samples.

Sample No	Growth Temperature (°C)	Seebeck Co-efficient (μV/ °C)	Electrical Conductivity (S/cm)	Power factor (mW/cmK²)
1	15	180-657	36-242	0.02-1.40
2	30	258-744	49-265	0.04-2.00
3	45	332-867	84-295	0.12-2.98
4	60	445-980	120-336	0.32-4.33

The values of the Seebeck coefficient were measured at different temperatures: 27°C, 47°C, 67°C, and 87°C, with a variation of 20°C after each measurement. It can be observed from Figure 14 that the values of the Seebeck coefficient (S) increase in relation to the bath temperature, which varies from 15°C to 60°C respectively, during the deposition of the films. The positive Seebeck values indicate the P-type semiconducting behavior of the material, which means the majority of charge carriers are holes [80]. Figure 9(a) also reveals a rise in Seebeck values as a function of temperature for all films, which is also affected by the growth temperature. The enhancement of Seebeck values for all samples with an increase in temperature is listed in table 2, and it is observed that a large number of carriers gain more thermal energy at higher temperatures. The excessive amount of Co atoms in the samples may create secondary phases, which increase the energy filtering effect at the grain level and result in higher Seebeck values. This effect refers to the trapping of energy carriers (where the excess charge carriers are holes) with low energy at grain boundaries or at the interfaces of two consecutive secondary phases. This filtering action is

an important facilitator in the improvement of carrier mobility, which enhances thermoelectric parameters such as the power factor and electrical conductivity [81, 82].

Electrical conductivity was also measured for all samples at different temperatures, shown in the figure 9(b). The enhancement in electrical conductivity was observed for higher temperatures listed in the table 2 this increment in the electrical conductivity with temperature indicates the semiconducting nature of the synthesized materials. Their electrical conductivity is shown below:

The improvement in the electrical conductivity is depending on the synthesis temperature, carrier concentration as well as carrier mobility. It can be seen from the Fig. 9(b) as the temperature rises electrical conductivity also increases for all samples listed in table 2. This enhancement in electrical conductivity is indicating that carrier concentration and carrier mobility in the samples is high, electrical conductivity is directly proportional to carriers' concentration. The increase in deposition temperature increases the deposition rate and increase in deposition means increase in number of secondary layers. These secondary layers of Zn^{+} & Co^{+} ions generate more holes as carriers and more carrier's concentration results in the enhancement of electrical conductivity [83, 84]. The electrical conductivity for the sample deposited at 15 ºC increases from 36 to 242 (Scm^{-1}) when temperature increase from 27 to 87 ºC, however the value of electrical conductivity for the sample deposited at 60 ºC increase from 120 to 336 (Scm^{-1}) same effect can be observed for all samples from the Table 2. This indicates that deposition temperature has a great influence on the electrical conductivity.

The value of power factor was calculated by the product of Seebeck co-efficient and electrical conductivity:

$$P = S^2\sigma$$

where **P** is power factor **S** is Seebeck co-efficient and **σ** is electrical conductivity of the synthesized materials.

The values of power factor depend upon the values of Seebeck co-efficient and electrical conductivity. The enhancement in the power is understandable due to the high values of Seebeck co-efficient and electrical conductivity (figure 9(c)). It can be observed that power factor is increasing with the increase of bath temperature [85].

4. Conclusions

In this research report, authors repotted the effect of synthesis method and temperature on the thermoelectric properties of $ZnCo_2O_4$ nanostructures. Zn-Co alloye films were deposited on Cu substrates by electrochemical deposition at different bath temperatures followed by hydrothermal oxidation of these alloy films at 100 ˚C. XRD patterns showed the formation of spinal structure of $ZnCo_2O_4$ nanostructures which was also confirmed by the Raman data as well. Optical data confirms the effect of deposition temperature on the band gap energies of the nanostructures which shows a red shift. The Seebeck coefficient value increased from 180-657 to 445-980 μV/ ˚C which exhibited a strong dependency on the increasing bath temperature.electrical conductivity and power factor also exhibited the same increasing patterns. The highest achieved power factor was for the sample which was deposited at 60˚C and showed a value of 4.33 mW/cmK^2. These values make this synthesis method a noval approach to achieve a material ($ZnCo_2O_4$) which could be a wonderful candidate for thermoelectric applications.

Acknowledgements

The authors would like to extend their sincere appreciation to the Researcher supporting program project number (RSPD2024R1114) King Saud University, Riyadh, Saudi Arabia.

References

[1] Narasimharao, K., M.M.M. Mostafa, Z.M. Al-Amshany, and W. Bajafar (2023), Catalysts 13:398; https://doi.org/10.3390/catal13020398

[2] Acosta, P.I., R.R. Campedelli, E.L. Correa, H.A. Bazani, E.N. Nishida, B.S. Souza, and J.R. Mora (2020), Fuel 271:117651; https://doi.org/10.1016/j.fuel.2020.117651

[3] Al-Zoubi, O.H., E.A.M. Saleh, A.N.A. Saieed, B.D. Olegovich, E.R. Alwaily, A. Alawadi, M. Talal, Y.F. Mustafa (2024), Materials Science in Semiconductor Processing 174:108234; https://doi.org/10.1016/j.mssp.2024.108234

[4] Dou, W., Y. Gong, X. Huang, Y. Li, Q. Zhang, Y. Liu, Q. Xia, Q. Jian, D. Xiang, D. Li (2024), Small 2311153; https://doi.org/10.1002/smll.202311153

[5] Wyżga, P., I. Veremchuk, P. Koželj, A. Leithe-Jasper, R. Gumeniuk (2021), Journal of Physics and Chemistry of Solids 152:109984; https://doi.org/10.1016/j.jpcs.2021.109984

[6] Nedunchezhian, A.A., D. Sidharth, R. Rajkumar, N.Y. Devi, K. Maeda, M. Arivanandhan, K. Fujiwara, G. Anbalagan, R. Jayavel (2020), RSC advances 10:18769-18775; https://doi.org/10.1039/D0RA01542C

[7] Nedunchezhian, A., D. Sidharth, R. Rajkumar, M.M. Ismail, M. Arivanandhan, I. Sarris, G. Anbalagan, R. Jayavel (2024), Journal of Inorganic and Organometallic Polymers and Materials 1-12; https://doi.org/10.1007/s10904-023-02972-7

[8] Li, J.-F., W.-S. Liu, L.-D. Zhao, M. Zhou (2010), NPG Asia Materials 2:152-158; https://doi.org/10.1038/asiamat.2010.138

[9] Pashkevich, A.V., A.K. Fedotov, E.N. Poddenezhny, L.A. Bliznyuk, V.V. Khovaylo, V.V. Fedotova, A.A. Kharchenko (2023), Modern Electronic Materials 9:45-56; https://doi.org/10.3897/j.moem.9.2.109827

[10] Ovik, R., B. Long, M. Barma, M. Riaz, M. Sabri, S. Said, R. Saidur (2016), Renewable and sustainable energy reviews 64:635-659; https://doi.org/10.1016/j.rser.2016.06.035

[11] Ren, P., Y. Liu, J. He, T. Lv, J. Gao, G. Xu (2018), Inorganic Chemistry Frontiers 5:2380-2398; https://doi.org/10.1039/C8QI00366A

[12] Zhou, M., G.J. Snyder, L. Li, L.-D. Zhao (2016), Inorganic Chemistry Frontiers 3:1449-1463; https://doi.org/10.1039/C6QI00263C

[13] Koumoto, K., Y. Wang, R. Zhang, A. Kosuga, R. Funahashi (2010), Annual review of materials research 40:363-394; https://doi.org/10.1146/annurev-matsci-070909-104521

[14] Hogarth, C., J. Andrews (1949) XXV, The London, Edinburgh, and Dublin Philosophical Magazine and Journal of Science 40:273-282; https://doi.org/10.1080/14786444908561249

[15] Hutson, A. (1959), Journal of Physics and Chemistry of Solids 8:467-472; https://doi.org/10.1016/0022-3697(59)90392-0

16. Parravano, G. (1955), The Journal of Chemical Physics 23:5-10; https://doi.org/10.1063/1.1740562

[17] Arvin, M. (1962), Phys. Chem. Solids 23; https://doi.org/10.1016/0022-3697(62)90252-4

[18] Frederikse, H., W. Thurber, W. Hosler (1964), Physical Review 134:A442; https://doi.org/10.1103/PhysRev.134.A442

[19] Thurber, W., A. Mante (1965), Physical Review 139:A1655; https://doi.org/10.1103/PhysRev.139.A1655

[20] Marley, J., R. Dockerty (1965), Physical Review 140:A304; https://doi.org/10.1103/PhysRev.140.A304

[21] Young, A., C. Schwartz (1969), Journal of Physics and Chemistry of Solids 30:249-252; https://doi.org/10.1016/0022-3697(69)90306-0

[22] Griffitbs, R., D. Elwell, R. Parker (1970), Phi1. Mag. 22:163-174; https://doi.org/10.1080/14786437008228161

[23] Bednorz, J.G., K.A. Müller (1986), Zeitschrift für Physik B Condensed Matter 64:189-193; https://doi.org/10.1007/BF01303701

[24] Cooper, J., B. Alavi, L. Zhou, W. Beyermann, G. Grüner (1987), Physical Review B 35:8794; https://doi.org/10.1103/PhysRevB.35.8794

[25] Chen, J., C. McEwan, L. Wenger, E. Logothetis (1987), Physical Review B 35:7124; https://doi.org/10.1103/PhysRevB.35.7124

[26] Lee, S., J. Lee, B. Suh, S. Moon, C. Lim, Z. Khim (1988), Physical Review B 37:2285; https://doi.org/10.1103/PhysRevB.37.2285

[27] Mitra, N., J. Trefny, B. Yarar, G. Pine, Z. Sheng, A. Hermann (1988), Physical Review B 38:7064; https://doi.org/10.1103/PhysRevB.38.7064

[28] Ohtaki, M., H. Koga, T. Tokunaga, K. Eguchi, H. Arai (1995), Journal of Solid State Chemistry 120:105-111; https://doi.org/10.1006/jssc.1995.1384

[29] Ohtaki, M., T. Tsubota, K. Eguchi, H. Arai (1996), Journal of applied physics 79:1816-1818; https://doi.org/10.1063/1.360976

[30] Terasaki, I., Y. Sasago, K. Uchinokura (1997), Physical Review B 56:R12685; https://doi.org/10.1103/PhysRevB.56.R12685

[31] Masset, A., C. Michel, A. Maignan, M. Hervieu, O. Toulemonde, F. Studer, B. Raveau, J. Hejtmanek (2000), Physical Review B 62:166; https://doi.org/10.1103/PhysRevB.62.166

[32] Funahashi, R., I. Matsubara, H. Ikuta, T. Takeuchi, U. Mizutani, S. Sodeoka (2000), Japanese Journal of Applied Physics 39:L1127; https://doi.org/10.1143/JJAP.39.L1127

[33] Okuda, T., K. Nakanishi, S. Miyasaka, Y. Tokura (2001), Physical Review B 63:113104; https://doi.org/10.1103/PhysRevB.63.113104

[34] Ohta, S., T. Nomura, H. Ohta, K. Koumoto (2005), Journal of applied physics 97; https://doi.org/10.1063/1.1847723

[35] Ohta, S., T. Nomura, H. Ohta, M. Hirano, H. Hosono, K. Koumoto (2005); Applied physics letters 87; https://doi.org/10.1063/1.2035889

[36] Fergus, J.W. (2012), Journal of the European Ceramic Society 32:525-540; https://doi.org/10.1016/j.jeurceramsoc.2011.10.007

[37] Acharya, M., S.S. Jana, M. Ranjan, T. Maiti (2021), Nano Energy 84:105905; https://doi.org/10.1016/j.nanoen.2021.105905

[38] Biswas, S., S. Singh, S. Singh, S. Chattopadhyay, K.K.H. De Silva, M. Yoshimura, J. Mitra, V.B. Kamble (2021), ACS Applied Materials & Interfaces 13:23771-23786; https://doi.org/10.1021/acsami.1c04125

[39] Zhang, Y., H. Ohta (2023), NPG Asia Materials 15:67; https://doi.org/10.1038/s41427-023-00520-w

[40] Xin, B., B. Paul, A. Le Febvrier, P. Eklund (2023), Materials Science in Semiconductor Processing 156:107300; https://doi.org/10.1016/j.mssp.2022.107300

[41] Jibri, K.M., J. Archana, M. Navaneethan, S. Harish (2023), Physical Chemistry Chemical Physics 25:12914-12922; https://doi.org/10.1039/D2CP04949J

[42] Assadi, M.H.N., J.J. Gutiérrez Moreno, M. Fronzi (2020), ACS Applied Energy Materials 3:5666-5674; https://doi.org/10.1021/acsaem.0c00640

[43] Sun, H., Y. Miao, G. Wang, X. Ren, E. Bao, X. Han, Y. Wang, X. Ma, C. Xu, H. Chen (2023), Journal of Energy Storage 72:108502; https://doi.org/10.1016/j.est.2023.108502

[44] Ya, M., Y. Wang, J. Wang, G. Gao, X. Zhao, Y. Wei, Z. Geng, G. Li, L. Li (2023), ACS Sustainable Chemistry & Engineering 11:15451-15459; https://doi.org/10.1021/acssuschemeng.3c04832

[45] Jheng, B.-R., P.-T. Chiu, S.-H. Yang, Y.-L. Tong (2022), Scientific reports 12:2921; https://doi.org/10.1038/s41598-022-06764-w

[46] Wang, J., B. Wang, A. Feng, Z. Jia, G. Wu (2020), Journal of Alloys and Compounds 834:155092; https://doi.org/10.1016/j.jallcom.2020.155092

[47] Tiwari, N., S. Kadam, S. Kulkarni (2021), Materials Letters 298:130039; https://doi.org/10.1016/j.matlet.2021.130039

[48] Munawar, T., S. Yasmeen, F. Mukhtar, M.S. Nadeem, K. Mahmood, M.S. Saif, M. Hasan, A. Ali, F. Hussain, F. Iqbal (2020), Ceramics International 46:14369-14383; https://doi.org/10.1016/j.ceramint.2020.02.232

[49] Munawar, T., F. Iqbal, S. Yasmeen, K. Mahmood, A. Hussain (2020), Ceramics International 46:2421-2437; https://doi.org/10.1016/j.ceramint.2019.09.236

[50] Yar, I.M., M. Irfan, F. Naheed, M.N. Akhtar, R.T. Rasool, G.A. Ashraf, S. Gulbadan, M.A. Khan (2024), Applied Physics A 130:87; https://doi.org/10.1007/s00339-023-07227-3

[51] Naheed, F., M. Irfan, S. Gulbadan, M.N. Akhtar, G.A. Ashraf, R.T. Rasool, M.A. Khan (2023) Materials Today Communications 35:106006; https://doi.org/10.1016/j.mtcomm.2023.106006

[52] Shanmugavalli, V., O. Saravanan, K. Vishista, R. Saravanan (2019), Ionics 25:4393-4408; https://doi.org/10.1007/s11581-019-02997-4

[53] Hamza, M., A. ur Rehman, I. Ali, M. Asif, M. Ahmad (2022), Journal of Magnetism and Magnetic Materials 564:169852; https://doi.org/10.1016/j.jmmm.2022.169852

[54] Schumacher, L.C., I.B. Holzhueter, I.R. Hill, M.J. Dignam (1990), Electrochimica acta 35:975-984; https://doi.org/10.1016/0013-4686(90)90030-4

[55] Alim, K.A., V.A. Fonoberov, M. Shamsa, A.A. Balandin (2005), Journal of Applied Physics 97:124313; https://doi.org/10.1063/1.1944222

[56] Sulciute, A., J. Baltrusaitis, E. Valatka (2015), Journal of Applied Electrochemistry 45:405-417; https://doi.org/10.1007/s10800-015-0802-7

[57] Samanta, K., P. Bhattacharya, R. Katiyar (2007), Physical Review B 75:035208; https://doi.org/10.1103/PhysRevB.75.035208

[58] Tortosa, M., M. Mollar, F. Manjón, B. Marí, J. Sánchez-Royo (2008), Physica Status Solidi C 5:3358-3360; https://doi.org/10.1002/pssc.200778857

[59] Saleem, M., A. Algahtani, S.U. Rehman, M.S. Javed, K. Irshad, H.M. Ali, M.Z. Malik, A. Ali, V. Tirth, S. Islam (2021), Nanomaterials 11:1710; https://doi.org/10.3390/nano11071710

[60] Roguai, S., A. Djelloul (2022), Solid State Communications 350:114740; https://doi.org/10.1016/j.ssc.2022.114740

[61] Li, J., X. Chen, N. Ai, J. Hao, Q. Chen, S. Strauf, Y. Shi (2011), Chemical Physics Letters 514:141-145; https://doi.org/10.1016/j.cplett.2011.08.048

[62] Hu, J., J. Cheng, S. Tong, Y. Yang, M. Chen, S. Hu (2016), International Journal of Photoenergy 2016; https://doi.org/10.1155/2016/2736257

[63] Eagen, C. (1981), Applied Optics 20:3035-3042; https://doi.org/10.1364/AO.20.003035

[64] Kumar, A., M. Jaiswal, D. Kanjilal, R.K. Joshi, T. Mohanty (2011), Applied Physics Letters 99; https://doi.org/10.1063/1.3608140

[65] Khan, M., N. Fatima, G.M. Mustafa, M. Sabir, S.A. Abubshait, H.A. Abubshait, T. Alshahrani, M. Iqbal, A. Laref, M. Baig (2021), International Journal of Energy Research 45:9685-9693; https://doi.org/10.1002/er.6469

[66] Barakat, N.A., M.S. Khil, F.A. Sheikh, H.Y. Kim (2008), The Journal of Physical Chemistry C 112:12225-12233; https://doi.org/10.1021/jp8027353

[67] Suwarnkar, M., R. Dhabbe, A. Kadam, K. Garadkar (2014); Ceramics International 40:5489-5496; https://doi.org/10.1016/j.ceramint.2013.10.137

[68] Gokul, B., P. Matheswaran, R. Sathyamoorthy (2013), Journal of Materials Science & Technology 29:17-21; https://doi.org/10.1016/j.jmst.2012.11.015

[69] Gençyılmaz, O., T. Taşköprü (2017), Journal of Alloys and Compounds 695:1205-1212; https://doi.org/10.1016/j.jallcom.2016.10.247

[70] Dhineshbabu, N.R., V. Rajendran, N. Nithyavathy, R. Vetumperumal (2016), Applied Nanoscience 6:933-939; https://doi.org/10.1007/s13204-015-0499-2

[71] Ur-Rehman, N., M. Mehmood, A.F. Khan, S.M. Ali, M. Ashraf (2020), Surface Review and Letters 27:1950149; https://doi.org/10.1142/S0218625X1950149X

[72] Chauhan, R., A.K. Srivastava, M. Mishra, K. Srivastava (2010), Integrated Ferroelectrics 119:22-32; https://doi.org/10.1080/10584587.2010.489496

[73] Swanepoel, R. (1983), Journal of Physics E: Scientific Instruments 16:1214; https://doi.org/10.1088/0022-3735/16/12/023

[74] Khan, H.N.-u.-R., M. Mehmood, F.C. Ling, A.F. Khan, S. Ali (2020), Semiconductors 54:999-1010; https://doi.org/10.1134/S1063782620090201

[75] Madhup, D., D. Subedi, S. Chimouriy (2010), J Optoelectron. Adv. M. **12**, 1035 (2010).

[76] Poudel, B., Q. Hao, Y. Ma, Y. Lan, A. Minnich, B. Yu, X. Yan, D. Wang, A. Muto, D. Vashaee (2008), Science 320:634-638; https://doi.org/10.1126/science.1156446

[77] Bell, L.E. (2008), Science 321:1457-1461; https://doi.org/10.1126/science.1158899

[78] Zheng, Z.-h., J.-t. Luo, F. Li, G.-x. Liang, P. Fan (2019); Current Applied Physics 19:470-474; https://doi.org/10.1016/j.cap.2019.01.019

[79] Nagaoka, A., K. Yoshino, T. Masuda, T.D. Sparks, M.A. Scarpulla, K. Nishioka (2021), Journal of Materials Chemistry A 9:15595-15604; https://doi.org/10.1039/D1TA02978A

[80] Oztan, C.Y., B. Hamawandi, Y. Zhou, S. Ballikaya, M.S. Toprak, R.M. Leblanc, V. Coverstone, E. Celik (2021), Journal of alloys and compounds 864:157916; https://doi.org/10.1016/j.jallcom.2020.157916

[81] Liu, M.-L., F.-Q. Huang, L.-D. Chen, I.-W. Chen (2009), Applied Physics Letters 94; https://doi.org/10.1063/1.3130718

[82] Ali, A., J. Jacob, A. Ashfaq, M. Tamseel, K. Mahmood, N. Amin, S. Hussain, W. Ahmad, U. Rehman, S. Ikram (2019), Ceramics International 45:12820-12824; https://doi.org/10.1016/j.ceramint.2019.03.202

[83] Ge, Z.-H., L.-D. Zhao, D. Wu, X. Liu, B.-P. Zhang, J.-F. Li, J. He (2016), Materials Today 19:227-239; https://doi.org/10.1016/j.mattod.2015.10.004

[84] Park, K. K. Ko (2007), Journal of alloys and compounds 430:200-204; https://doi.org/10.1016/j.jallcom.2006.04.065

[85] Liu, M.L., I.W. Chen, F.Q. Huang, L.D. Chen (2009), Advanced Materials 21:3808-3812; https://doi.org/10.1002/adma.200900409